Organic Electronics 13 (2012) 560–569

Contents lists available at SciVerse ScienceDirect

Organic Electronics

journal homepage: www.elsevier.com/locate/orgel

Porphyrins modified with a low-band-gap chromophore for dye-sensitized solar cells

Weiping Zhou [a], Zhencai Cao [a], Shenghui Jiang [a], Hongyan Huang [a], Lijun Deng [a], Yijiang Liu [a], Ping Shen [a], Bin Zhao [a], Songting Tan [a,*], Xianxi Zhang [b,*]

[a] College of Chemistry, Key Laboratory of Advanced Functional Polymeric Materials, Xiangtan University, Xiangtan 411105, PR China
[b] Shandong Provincial Key Laboratory of Chemical Energy Storage and Novel Cell Technology, School of Chemistry and Chemical Engineering, Liaocheng University, Liaocheng 252059, China

ARTICLE INFO

Article history:
Received 18 October 2011
Received in revised form 16 December 2011
Accepted 28 December 2011
Available online 10 January 2012

Keywords:
Dye-sensitized solar cells
Low-band-gap chromophore
Photovoltaic performance
Porphyrins

ABSTRACT

Two novel porphyrin dyes (**PMBTZ** and **PHBTZ**) modified with alkyl-thiophene and 2,1,3-benzothiadiazole (BTZ) moieties were designed and synthesized. The optical and electrochemical properties were characterized by UV–visible, fluorescence spectroscopy and cyclic voltammetry. With the introduction of the low-band-gap chromophore onto the porphyrins, the absorption spectra of the two porphyrin dyes in the range of 450–600 nm were broadened and the maximum wavelength was red-shifted compared with $\mathbf{P_{Zn}}$ as expected. The first oxidation potentials (E_{ox1}) were altered to the negative, which lowered from 1.27 to 1.11 and 1.15 eV, respectively. For a typical solar cell device based on dye **PMBTZ**, the maximal monochromatic incident photon-to-current conversion efficiency (IPCE) can reach to 65%, with a broad respondent region of 350–800 nm. Under standard global AM 1.5 solar condition, the dye-sensitized solar cell (DSSC) based on the dye **PMBTZ** showed the best photovoltaic performance: a short-circuit photocurrent density (J_{sc}) of 14.11 mA/cm^2, an open-circuit photo voltage (V_{oc}) of 0.59 V, and a fill factor (*ff*) of 0.66, corresponding to solar-to-electric power conversion efficiency (η) of 5.46%.

1. Introduction

In recent years renewable energy sources are under intense study due to global warming and increasing energy demands. The solar-to-electric energy conversion is likely to play a key role in replacing fossil fuels. And then, tremendous research efforts have been devoted to dye-sensitized solar cells (DSSCs) to seek cost-effective and resource-unlimited photovoltaic devices [1]. To date, the Ru-polypyridyl complexes utilized by Grätzel proved to be the most efficient TiO_2-sensitizers with the N3 dye showing an overall photovoltaic cell energy conversion efficiency of 11% [2]. Although this efficiency is half of the traditional silicon based cells, it is still high enough for practical utility.

But then, with a view to the limited ruthenium resource, metal-free organic dyes have attracted considerable attention in recent years owing to their excellent flexibility in terms of molecular tailoring and high molar absorption coefficients due to intramolecular π–π^* transitions. In the past years, various metal-free dyes such as coumarin [3], indoline [4], perylene [5], merocyanine [6], porphyrin [7], triarylamine [8], and carbazole [9] have been reported, all of which have obtained power conversion efficiency in the range of 5–9%.

Recently, porphyrins have been recognized as promising components of molecular electronic and photonic devices [10] because of their photochemical and electrochemical stabilities, strong absorbing ability in the visible region due to π–π^* transitions of the conjugated macrocycle and high molar extinction coefficients [11]. They show ultrafast electron injection and slow charge recombination kinetics which are indistinguishable to those of N3 dye [12], one of the most efficient photosensitizers ever reported. However,

* Corresponding authors.
E-mail addresses: tanst2008@163.com (S. Tan), zhangxianxi@lcu.edu.cn (X. Zhang).

1566-1199/$ - see front matter © 2011 Elsevier B.V. All rights reserved.
doi:10.1016/j.orgel.2011.12.014

the narrow light absorption spectra of porphyrins, which poorly match to solar light distribution, resulted in inferior performances as compared with ruthenium polypyridyl complexes applied in DSSCs. A strategy to solve this problem is to make the strong and narrow Soret-band broad and weak Q-bands strong by extension of the porphyrin π-system by modifying a β-position [13]. For example, Seunghun et al. synthesized β,β′-quinoxalino porphyrins containing carboxylic acid binding groups employed for dye-sensitized solar cells, which showed broadened and red-shifted light absorption with the aid of π-extensions. The DSSC based on porphyrin dye exhibited power conversion efficiencies of 5.2% [14]. The Grätzel group and the Officer group showed that a combination of a conjugated diethenyl linker at the β-pyrrolic position with a carboxylate binding group improves cell performance and gives a cell efficiency of 7.1% [15]. Diau group and the Yeh group reported novel porphyrin molecules with carboxylic acid binding groups at *meso*-positions connected with a phenylethynyl bridge co-adsorbed with chenodioxycholic acid (CDCA) on TiO_2, giving an excellent cell efficiency of 11% [16]. Theoretical calculations were also used in design and screening of promising porphyrin sensitizer candidates, and interpreting the performance differences of porphyrin-sensitized solar cells, which provided further assistance to the experimental researches [17].

In our previous reports, a successful approach was introduced by incorporating thiophene moieties into the organic framework, which not only achieved high conversion efficiency of 5.14% but also revealed that the linker between donor and accepter could not be too long [11e]. To further improve the photovoltaic performance of this system, an enhanced spectral response of the sensitizer in the red region is required. In this article, we designed and synthesized two dyes based on porphyrins modified with thiophene and 2,1,3-benzothiadiazole (BTZ) moieties as shown in Fig. 1, which were then applied in DSSCs. Density functional theory (DFT) calculations of the dyes were also performed to help interpreting the performances of corresponding solar cells. The introduction of low-band-gap chromophore in the bridging framework is presumed to increase the spectral response in the red portion of the solar spectrum [18]. The alkyl groups on the thiophenes were aimed to reduce charge recombination and improve the solubility of the dyes in solutions to some extent.

2. Experimental details

2.1. Materials and reagents

All starting materials were purchased from Pacific ChemSource and Alfa Aesar. DMF, $HCCl_3$, MeCN and $POCl_3$ were dried and distilled by accustomed methods. All other solvents and chemicals used in this work were analytical grade and used without further purification. All chromatographic separations were carried out on silica gel (200–300 mesh).

2.2. Analytical instruments

^1H and ^{13}C NMR spectra were recorded with a Bruker Avance 400 instrument. Element analyzes were measured by an Elementar Vario EL III element analyzer. UV–visible spectra of the dyes were measured on a Perkin–Elmer Lamada 25 spectrometer. The PL spectra were obtained using Perkin–Elmer LS-50 luminescence spectrometer. MALDI-TOF mass spectrometric measurements were performed on Bruker Bifiex III MALDI-TOF. Electrochemical redox potentials were obtained by cyclic voltammetry (CV) using a three-electrode configuration and an electrochemistry workstation (ZAHNER ZENNIUM). The working electrode was a glassy carbon electrode; the auxiliary electrode was a Pt electrode, and saturated calomel electrode (SCE) was used as reference electrode. Tetrabutylammonium hexafluorophosphate 0.1 M was used as supporting electrolyte in dry DMF. Ferrocene was added to each sample solution at the end of the experiments, and was used as an internal potential reference.

2.3. General procedure for preparation of porphyrin-modified TiO_2 electrode and photovoltaic measurements

Fluorine-doped SnO_2 conducting glass (FTO) were cleaned and immersed in aqueous 40 mM $TiCl_4$ solution at 70 °C for 30 min, then washed with water and ethanol, sintered at 450 °C for 30 min. The 20–30 nm particles sized TiO_2 colloid blended with 0.1 wt.% magnesium acetate solution was coated onto the FTO glass by sliding glass rod method to obtain a TiO_2 film of 10–15 μm thickness after drying. The 200 nm particles sized TiO_2 colloid was coated on the electrode by the same method, resulting in

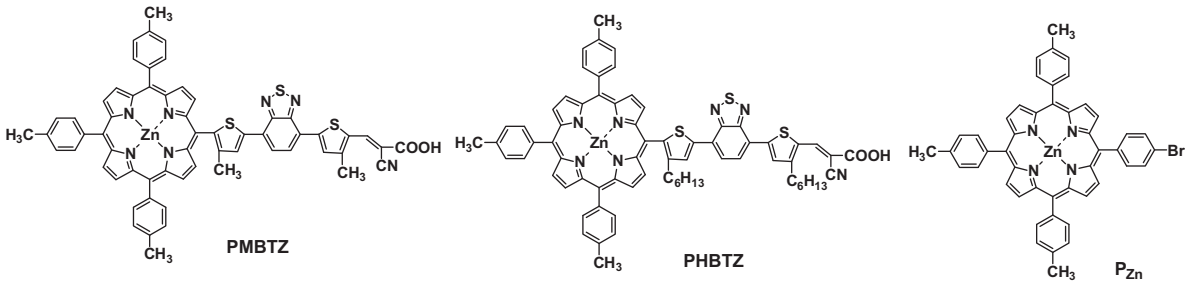

Fig. 1. Molecular structures of porphyrin dyes and $\mathbf{P_{Zn}}$.

a TiO_2 light-scattering layer of 4–6 μm thickness. The TiO_2 electrodes were immersed into each of the 1 mM DMF solution of the porphyrins at room temperature. After dye adsorption, the dye-coated electrodes were copiously rinsed with ethanol. The amounts of the porphyrins adsorbed on the TiO_2 films were determined by measuring absorbance at the Soret-band of the dye molecules that were dissolved from the dye-adsorbed TiO_2 films into DMF/H_2O (4:1) containing 0.1 M NaOH. The photovoltaic measurements were performed in a sandwich cell consisting of the porphyrin-sensitized TiO_2 electrode as the working electrode and a Pt foil as the counter electrode. The electrolyte consists of 0.5 M LiI, 0.05 M I_2, and 0.5 M 4-*tert*-butylpyridine (TBP) in 3-methoxypropionitrile and the efficient irradiated area of cell was 0.196 cm^2. The photocurrent–voltage (*J*–*V*) characteristics were measured with a Keithley 2602 Source meter under the 100 mW cm^{-2} irradiation of a 500 W Xe lamp with a global AM 1.5 filter for solar spectrum simulation. The solar-to-electricity conversion efficiency (η) of the DSSCs is calculated from short-circuit photocurrent (J_{sc}), the open-circuit photovoltage (V_{oc}), the fill factor (*ff*) and the intensity of the incident light (P_{in}) according to the following equation:

$$\eta = \frac{J_{SC}(\text{mA cm}^{-2}) \times V_{OC}(V) \times ff}{P_{in}(\text{mW cm}^{-2})}$$

The IPCE values are plotted as a function of the excited wavelength and defined according to the following equation:

$$\text{IPCE}(\lambda) = \frac{1240}{\lambda(\text{nm})} \times \frac{J_{SC}(\text{mA cm}^{-2})}{\Phi(\text{mW cm}^{-2})}$$

where J_{sc} is the short-circuit photocurrent density generated by monochromatic light, λ is the wavelength of incident monochromatic light, and Φ is the incident light intensity.

2.4. The detailed experimental procedures and characterization data

2.4.1. 2-(tri-n-Butylstannyl)-4-methylthiophene (**1-a**)

Under argon atmosphere, 3-methylthiophene (1.96 g, 20 mmol) and 50 mL freshly distilled dry THF were added in a 100 mL three-necked flask. *n*-Butyllithium (8.8 mL, 2.5 M in hexane, 22 mmol) was added dropwise at −78 °C, and the solution was stirred for 1 h at −78 °C, then tributyltin chloride (6 mL, 22 mmol) was added. The mixture was allowed up to room temperature slowly and stirred for another 24 h. Finally, the mixture was poured into 100 mL cooled water, and extracted by hexane. The organic layer was dried over anhydrous $MgSO_4$. Removal of the solvent by rotary evaporation, a yellow–brown liquid **1-a** (7.12 g, 85%) was obtained. The crude product was used in next step without further purification. ^{1}H NMR ($CDCl_3$, 400 MHz, δ/ppm): 7.20 (s, 1H, thienyl-H), 6.97 (s, 1H, thienyl-H), 2.33 (t, 3H, –CH_3), 1.64–1.54 (m, 6H, –CH_2), 1.40–1.31 (m, 6H,–CH_2), 1.19–1.08 (m, 6H, –CH_2), 0.95–0.90 (m, 9H, –CH_3).

2.4.2. 4,7-bis-(4-Methylthiophen-2-yl)benzo[1,2,5]thiadiazole (**2-a**)

4,7-Dibromo-2,1,3-benzothiadiazole (1 g, 3.4 mmol) and **1-a** (2.85 g, 6.8 mmol), $Pd(PPh_3)_4$ (0.084 g, 0.075 mmol), were dissolved in toluene (50 mL) and the mixture was refluxed for 48 h. After evaporating the solvent under reduced pressure, H_2O (50 mL) and chloride (50 mL) were added. The organic layer was separated and dried over anhydrous $MgSO_4$. The solvent was removed under reduced pressure. The pure product **2-a** was obtained as orange solid by column chromatography on silica gel (CH_2Cl_2/hexane = 1/8). Yield: 0.86 g, 78%. ^{1}H NMR ($CDCl_3$, 400 MHz, δ/ppm): 7.97 (s, 2H, thienyl-H), 7.84 (s, 2H, phenyl-H), 7.05 (s, 2H, thienyl-H), 2.39 (s, 6H, –CH_3).

2.4.3. [(3-Methylthiophen-2-yl)benzo[1,2,5]thiadiazol-4-yl]-4-methylthiophene-2-carbaldehyde (**3-a**)

In a 100 mL three-necked flask, **2-a** (2.1 g, 6.4 mmol), DMF (0.6 mL, 7.7 mmol), 1,2-dichloroethane 50 mL were added sequentially under Ar atmosphere and $POCl_3$ (0.7 mL, 7.7 mmol) was added quickly at 0 °C. The mixture was heated to 80 °C and stirred for 12 h. After cooling to room temperature, poured into sodium acetate solution and stirred for an additional 1 h. The solution was extracted with dichloromethane, and washed with H_2O and brine. The organic layer was dried over anhydrous $MgSO_4$. Solvent was removed by rotary evaporation, and the residue was purified by silica gel column chromatography with petroleum ether/dichloromethane = 1/1 as eluent to yield **3-a** as an orange–red solid. Yield: 1.64 g, 72%.^{1}H NMR ($CDCl_3$, 400 MHz, δ/ppm): 10.11 (s, 1H, –CHO), 8.07–8.02 (s, 2H, phenyl-H), 7.97–7.95 (d, 1H, thienyl-H), 7.88–7.86 (d, 1H, thienyl-H), 7.10 (s, 1H, thienyl-H), 2.68 (s, 3H, –CH_3), 2.39 (s, 3H, –CH_3).

2.4.4. [(4-Methylthiophen-2-yl)benzo[1,2,5]thiadiazol-4-yl]-4-methylthiophene-2-10,15,20-tris(4-methylphenyl) porphyrin (**4-a**)

In a 250 mL three-necked round-bottomed flask, **3-a** (2.73 g, 7.66 mmol), 4-methylbenzaldehyde (3.17 g, 26.3 mmol) were dissolved in 200 mL propionic acid. The solution was heated to reflux at 140 °C. Pyrrole (2.44 mL, 30.7 mmol) was added dropwise and stirred for another 2 h. After cooling to room temperature (rt), the solvent was evaporated. The crude production was separated by column chromatography (petroleum ether/dichloromethane = 3/1 as an eluent). After recrystallization from CH_3OH, the desired bright purple solid compound **4-a** was obtained. Yield: 0.84 g, 12.1%. ^{1}H NMR ($CDCl_3$, 400 MHz, δ/ppm): 9.11–8.87 (m, 8H, pyrrol-H), 8.50–8.48 (m, 2H, phenyl-H), 8.12–8.05 (m, 10H, phenyl-H), 7.59–7.57 (m, 4H, aryl-H), 7.08(s, 1H, thienyl-H), 2.72 (s, 9H, –CH_3), 2.42 (s, 3H, –CH_3), 2.26 (s, 3H, –CH_3), −2.64 (s, 2H, N–H). MALDI-TOF MS ($C_{57}H_{42}N_6S_3$) *m*/*z*: calcd for 907.293; found 907.285.

2.4.5. [(4-Methylthiophen-5-formyl-2-yl)benzo[1,2,5]thiadiazol-4-yl]-4-methylthiophene-2-10,15,20-tris(4-methyl phenyl) porphyrin (**5-a**)

In a 50 mL three-necked flask, porphyrin **4-a** (0.55 g, 0.6 mmol), DMF (1.62 mL, 20 mmol), 1,2-dichloroethane 25 mL were added sequentially under Ar atmosphere and $POCl_3$ (1.88 mL, 20 mmol) was added quickly at 0 °C. The

mixture was heated to 80 °C and stirred for 12 h. After cooling to room temperature, the mixture was poured into sodium acetate solution and stirred for an additional 1 h. The solution was extracted with dichloromethane, and washed with H_2O and brine. The organic layer was dried over anhydrous $MgSO_4$. Solvent was removed by rotary evaporation, and the residue was purified by silica gel column chromatography with petroleum ether/dichloromethane = 1/1 as eluent to yield **5-a** (0.24 g, 42.8%) as a purple–red solid. ^{1}H NMR ($CDCl_3$, 400 MHz, δ/ppm):10.14 (s, 1H, –CHO), 9.06–8.87 (m, 8H, pyrrol-H), 8.53 (s, 1H, aryl-H), 8.14–8.05 (m, 10H, phenyl-H), 7.59–7.57 (m, 5H, aryl-H), 2.72 (s, 9H, $-CH_3$), 2.71 (s, 3H, $-CH_3$), 2.26 (s, 3H, $-CH_3$), −2.65 (s, 2H, N–H). MALDI-TOF MS ($C_{58}H_{42}N_6S_3O$) *m*/*z*: calcd for 935.198; found 935.252.

*2.4.6. [(4-Methylthiophen-5-formyl-2-yl)benzo[1,2,5] thiadiazol-4-yl]-4-methylthiophene-2-10,15,20-tris (4-methylphenyl) porphyrin zinc (**6-a**)*

A mixture of **5-a** (0.24 g, 0.25 mmol) and Zn $(OAc)_2$ (0.18 g, 1 mmol) in $CHCl_3$ (50 mL) and CH_3OH (10 mL) was refluxed for 4 h. After cooling to room temperature, the mixture was washed with H_2O. The organic layer was dried over anhydrous $MgSO_4$ and concentrated by rotary evaporation. A purple with a little green solid of compound **6-a** was obtained. Yield: 0.23 g, 93.7%. ^{1}H NMR ($CDCl_3$, 400 MHz, δ/ppm): 10.13 (s, 1H, –CHO), 9.06–8.89 (m, 8H, pyrrol-H), 8.53 (s, 1H, aryl-H), 8.12–8.05 (m, 10H, phenyl-H), 7.59–7.57 (m, 5H, aryl-H), 2.72 (s, 9H, $-CH_3$), 2.26 (s, 3H, $-CH_3$), 2.71(s, 3H, –CH3).

*2.4.7. 2-Cyano-3-(3-methyl-5-(4-(10,15,20-tris(4-methyl phenyl))porphyrinatozinc (II)yl)-3-methyl-5-benzo[1,2,5] thiadiazol-4-yl)thienyl acrylic acid (**7-a**)*

To a solution of acetonitrile (15 mL) and toluene (5 mL), porphyrin compound **6-a** (0.20 g, 0.20 mmol), cyanoacetic acid (0.073 g, 0.87 mmol) and piperidine (0.5 mL) were added sequentially under Ar atmosphere. The mixture was refluxed for 16 h. After cooling to room temperature, the solution was extracted with dichloromethane, and washed with H_2O and 0.1 M HCl. The organic layer was dried over anhydrous $MgSO_4$. Solvent was removed by rotary evaporation, and the residue was purified by silica gel column chromatography with methanol/dichloromethane (1/20) as eluent to yield a purple solid with a little green compound **7-a**. Yield: 0.095 g, 42%. ^{1}H NMR ($CDCl_3$, 400 MHz, δ/ppm): 9.17–8.97 (m, 8H, pyrrol-H), 8.55 (s, 1H, aryl-H), 8.52 (s, 1H, vinyl-H), 8.13 (m, 10H, phenyl-H), 7.57 (m, 5H, aryl-H), 2.72–2.60 (m, 15H, $-CH_3$). ^{13}C NMR (DMSO, 400 MHz, ppm): 152.2, 150.6, 150.2, 150.0, 149.6, 140.6, 138.4, 136.9, 134.5, 134.3, 134.1, 132.6, 132.5, 131.9, 131.7, 131.6, 131.3, 131.1, 139.9, 129.6, 128.1, 127.9, 127.8, 127.6, 127.2, 127.0, 125.6, 125.3, 125.1, 124.7, 124.5, 123.7, 121.6, 121.1, 14.3. MALDI-TOF MS ($C_{61}H_{41}N_7S_3O_2Zn$) *m*/*z*: calcd for 1063.179; found 1063.181. Anal calcd for $C_{61}H_{41}N_7O_2S_3Zn$: C, 68.79; H, 3.85; N, 9.21; S, 9.02%. Found: C, 68.34; H, 4.05; N, 8.19; S, 8.16%.

*2.4.8. 2-(tri-n-Butylstannyl)-4-hexylthiophene (**1-b**)*

The product **1-b** was prepared using the same procedure for **1-a** except that 3-hexylthiophene was used instead of 3-methylthiophene. Yield:7.82 g, 85%. ^{1}H NMR ($CDCl_3$, 400 MHz, δ/ppm): 7.18 (s, 1H, thienyl-H), 6.96 (s, 1H, thienyl-H), 2.82–2.80 (t, 2H, $-CH_2$), 1.70–1.62 (m, 2H, $-CH_2$), 1.60–1.55 (m, 8H, $-CH_2$), 1.36–1.30 (m, 8H, $-CH_2$), 1.11–1.06 (m, 8H, $-CH_2$), 0.93–0.87 (m, 12H, $-CH_3$).

*2.4.9. 4,7-bis-(4-Hexylthiophen-2-yl)benzo[1,2,5]thiadiazole (**2-b**)*

The product **2-b** was prepared using the same procedure for **2-a** except that **1-b** was used instead of **1-a**. Yield: 1.08 g, 68%. ^{1}H NMR ($CDCl_3$, 400 MHz, δ/ppm): 7.99 (s, 2H, thienyl-H), 7.84 (s, 2H, phenyl-H), 7.06 (s, 2H, thienyl-H), 2.71 (t, 4H, $-CH_2$), 1.72–1.60 (m, 8H, $-CH_2$), 1.36–1.22 (m, 8H, $-CH_2$), 0.94 (t, 6H, $-CH_3$).

*2.4.10. [(3-Hexylthiophen-2-yl)benzo[1,2,5]thiadiazol-4-yl]-4-hexylthiophene-2-carbaldehyde (**3-b**)*

The product **3-b** was prepared using the same procedure for **3-a** except that **2-b** was used instead of **2-a**. Yield: 2.5 g, 78%. 1H NMR ($CDCl_3$, 400 MHz, δ/ppm): 10.11(s, 1H, –CHO), 8.07–8.05 (d, 2H, phenyl-H), 7.98–7.96 (d, 1H, thienyl-H), 7.89–7.87 (d, 1H, thienyl-H), 7.11 (s, 1H, thienyl-H), 3.07–3.03 (t, 2H, $-CH_2$), 2.74–2.70 (t, 2H, $-CH_2$), 1.81–1.70 (m, 4H, $-CH_2$), 1.43–1.36 (m, 12H, $-CH_2$), 0.93–0.92 (t, 6H, $-CH_3$).

*2.4.11. [(4-Hexylthiophen-2-yl)benzo[1,2,5]thiadiazol-4-yl]-4-hexylthiophene-2-10,15,20-tris(4-methylphenyl) porphyrin (**4-b**)*

The product **4-b** was prepared using the same procedure for **4-a** except that **3-b** was used instead of **3-a**. (1.02 g, 12.7%). ^{1}H NMR ($CDCl_3$, 400 MHz, δ/ppm): 9.10–8.85 (m, 8H, pyrrol-H), 8.52–8.05 (m, 12H, phenyl-H), 7.81–7.56 (m, 4H, aryl-H), 7.08 (s, 1H, thienyl-H), 2.76–2.65 (s, 9H, $-CH_3$), 2.64–2.49 (t, 4H, $-CH_2$), 1.77–1.65 (m, 4H, $-CH_2$), 1.41–1.25 (m, 12H, $-CH_2$), 0.54–0.52 (t, 6H, $-CH_3$), −2.65 (s, 2H, N–H).

*2.4.12. [(4-Hexylthiophen-5-formyl-2-yl)benzo[1,2,5]thiadiazol-4-yl]-4-hexylthiophene-2-10,15,20-tris(4-methylphenyl) porphyrin (**5-b**)*

The product **5-b** was prepared using the same procedure for **5-a** except that **4-b** was used instead of **4-a**. Yield: 0.25 g, 45.9%. ^{1}H NMR ($CDCl_3$, 400 MHz, δ/ppm):10.12 (s, 1H, –CHO), 9.06–8.85 (m, 8H, pyrrol-H), 8.56–8.05 (m, 12H, phenyl-H), 7.81–7.77 (s, 1H, thienyl-H), 7.56–7.55 (m, 3H, aryl-H), 3.08–3.06 (t, 2H, $-CH_2$), 2.96–2.70 (m, 9H, $-CH_3$), 2.57–2.53 (t, 2H, $-CH_2$), 2.06–2.00 (t, 2H, $-CH_2$), 1.82–1.76 (t, 2H, $-CH_2$), 1.45–1.25 (m, 12H, $-CH_2$), 0.93–0.83 (t, 3H, $-CH_3$), 0.53–0.50 (t, 3H, $-CH_3$), −2.65–2.69 (s, 2H, N–H). MALDI-TOF MS ($C_{68}H_{62}N_6S_3O$) *m*/*z*: calcd for 1075.406; found 1075.319.

*2.4.13. [(4-Hexylthiophen-5-formyl-2-yl)benzo[1,2,5]thiadiazol-4-yl]-4-hexylthiophene-2-10,15,20-tris(4-methylphenyl) porphyrin zinc (**6-b**)*

The product **6-b** was prepared using the same procedure for **6-a** except that **5-b** was used instead of **5-a**. Yield: 0.55 g, 95%. ^{1}H NMR ($CDCl_3$, 400 MHz, δ/ppm):10.12 (s, 1H, –CHO), 9.06–8.85 (m, 8H, pyrrol-H), 8.56–8.05 (m, 12H, phenyl-H), 7.81–7.77 (s, 1H, thienyl-H), 7.56–7.55 (m, 3H, aryl-H), 3.08–3.06 (t, 2H, $-CH_2$), 2.96–2.70 (m, 9H, $-CH_3$),

2.57–2.53 (t, 2H, $-CH_2$), 2.06–2.00 (t, 2H, $-CH_2$), 1.82–1.76 (t, 2H, $-CH_2$), 1.45–1.25 (m, 12H, $-CH_2$), 0.93–0.83(t, 3H, $-CH_3$), 0.53–0.50 (t, 3H, $-CH_3$).

*2.4.14. 2-Cyano-3-(3-hexyl-5-(4-(10,15,20-tris(4-methyl phenyl))porphyrinatozinc (II)yl)-3-hexyl-5-benzo[1,2,5] thiadiazol-4-yl)thienyl acrylic acid (**7-b**)*

The product **7-b** was prepared using the same procedure for **7-a** except that **6-b** was used instead of **6-a**. Yield: 0.12 g, 34.8%. ^{1}H NMR ($CDCl_3$, 400 MHz, δ/ppm): 9.06–8.85 (m, 8H, pyrrol-H), 8.57 (s, 1H, vinyl-H), 8.38–8.05 (m, 12H, phenyl-H), 7.81–7.77 (s, 1H, thienyl-H), 7.56–7.55 (m, 3H, aryl-H), 3.08–3.06 (t, 2H, $-CH_2$), 2.96–2.70 (m, 9H, $-CH_3$), 2.57–2.53 (t, 2H, $-CH_2$), 2.06–2.00 (t, 2H, $-CH_2$), 1.82–1.76 (t, 2H, $-CH_2$), 1.45–1.25 (m, 12H, $-CH_2$), 0.93–0.83(t, 3H, $-CH_3$), 0.53–0.50 (t, 3H, $-CH_3$). ^{13}C NMR (DMSO, 400 MHz, ppm): 152.2, 150.8, 150.2, 150.0, 149.6, 140.1, 138.2, 137.0, 134.8, 134.6, 134.4, 132.6, 132.5, 132.1, 131.9, 131.8, 131.6, 131.3, 130.0, 129.9, 128.0, 127.9, 127.8, 127.7, 127.2, 127.1, 125.6, 125.5, 125.1, 124.7, 124.5, 123.9, 121.9, 121.1, 34.2, 31.4, 29.4, 28.8, 25.0, 22.1, 14.3. MALDI-TOF MS ($C_{71}H_{61}N_7S_3O_2Zn$) m/z: calcd for 1203.332; found 1203.325. Anal calcd for $C_{71}H_{61}N_7O_2S_3Zn$: C, 70.76; H, 5.06; N, 8.14; S,7.97%. Found: C, 69.21; H, 5.28; N, 7.25; S, 7.26%.

3. Results and discussion

3.1. Synthesis and characterization

The two dyes have been synthesized according to several classical reactions. The synthetic strategy is shown in Scheme 1. Taking **PMBTZ** as example, the dye was synthesized as following steps. First, 2-(tri-*n*-butylstannyl)-4-methylthiophene **1-a**, was obtained from 3-methylthiophene in the presence of *n*-BuLi and tributyltin chloride. Then the compound **3-a** was obtained by two steps: (1) 4,7-bis-(4-methylthiophen-2-yl)benzo[1,2,5]thiadiazole (**2-a**) was synthesized by Stille coupling with 4,7-dibromo-2,1,3-benzothiadiazole and **1-a**; (2) then **2-a** reacted via Vilsmeier formylation reaction with $POCl_3$ and DMF in 1,2-dichloroethane to get **3-a**. The key intermediate **4-a** was obtained by Adler-Longo method with **3-a** and 4-methylbenzaldehyde and pyrrole. Subsequently, **4-a** was converted into compound **5-a** by Vilsmeier formylation. Finally, compound **5-a** was treated with $Zn(OAc)_2$ to get **6-a**, and then reacted with cyanoacetic acid by Knoevenagel reaction to give **PMBTZ**. And **PHBTZ** was synthesized by the same procedure as that for **PMBTZ** except that 3-hexylthiophene was used instead of 3-methylthiophene. The structures of

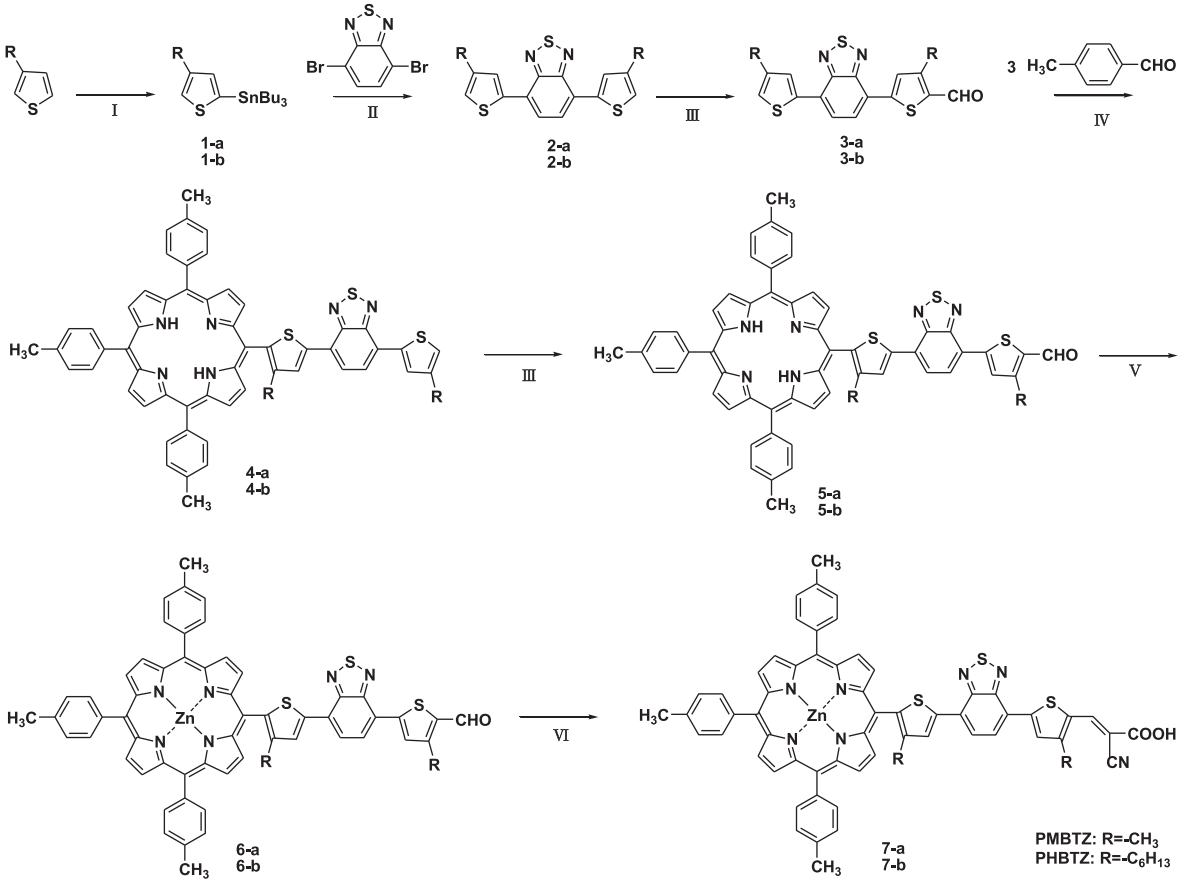

Scheme 1. The synthetic strategy of monomers and the two dyes. Reagents and conditions: I: (1) *n*-BuLi, THF, −78 °C, (2) tributyltin dichloride; II: $Pd(PPh_3)_4$, toluene; III: $POCl_3$, DMF, 1,2-dichloroethane; IV: pyrrole, propionic acid; V: $Zn(OAc)_2$, CH_3OH, $CHCl_3$; VI: cyanoacetic acid, piperdine, CH_3CN.

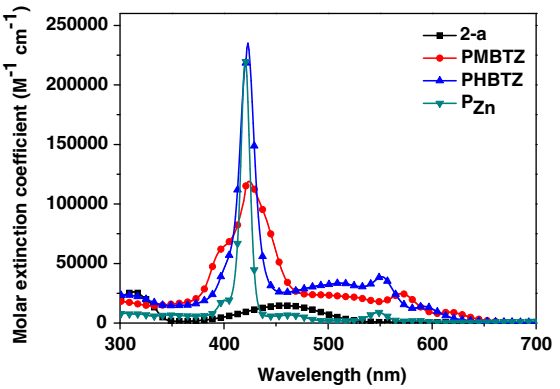

Fig. 2. Absorption spectra of porphyrin dyes and **2-a** in $CHCl_3$ solutions.

the two dyes were verified by ^1H NMR, ^{13}C NMR, and MALDI-TOF mass spectra.

3.2. Optical properties

Fig. 2 shows the absorption spectra of sensitizers (**PMBTZ** and **PHBTZ**), reference $\mathbf{P_{Zn}}$ and low-band-gap chromophore (**2-a**) measured in $CHCl_3$ solutions. The data are listed in Table 1. The compound **2-a** exhibits two strong absorption bands at 313 nm ($\varepsilon = 2.6 \times 10^4\ M^{-1}\ cm^{-1}$) and 458 nm ($\varepsilon = 1.4 \times 10^4\ M^{-1}\ cm^{-1}$). $\mathbf{P_{Zn}}$ exhibits a strong but narrow absorption peak located at 420 nm and weak Q-bands at 547 ($\varepsilon = 7 \times 10^3\ M^{-1}\ cm^{-1}$) and 586 nm, which are attributed to π–π^* electron transition. After modification, the synthesized porphyrin dyes obtain improved spectra as shown in Fig. 2, which is broadened in Soret-bands and strengthened in Q-bands.

The shape and the peak positions of the spectra are analogous for **PMBTZ** and **PHBTZ**. The two dyes both exhibit strong Soret – at 424 ($\varepsilon = 1.19 \times 10^5\ M^{-1}\ cm^{-1}$) and 423 nm ($\varepsilon = 2.35 \times 10^5\ M^{-1}\ cm^{-1}$), and moderate Q-bands. After modification with the low-band-gap chromophore on the linker, the Soret-bands of the two dyes are much broader and red-shifted than $\mathbf{P_{Zn}}$. It is obvious that the spectrum of **PMBTZ** at the Soret-band with a shoulder is broader than that of **PHBTZ** which is attributed to the *J*-aggregation. And the Q-bands of the two dyes are much stronger than $\mathbf{P_{Zn}}$. Corresponding molar extinction coefficients of the two dyes at Q-bands are 2.5×10^4 and $3.8 \times 10^4\ M^{-1}\ cm^{-1}$, respectively, which is 3–5 folder than $\mathbf{P_{Zn}}$. And the absorption in the range between Soret-band and Q-bands was improved evidently. On the other hand, the blue-shift of **PHBTZ** compared to **PMBTZ** can be readily interpreted by the molecular modeling study of the two sensitizers. The optimized structures of the two porphyrin dyes calculated at density functional B3LYP/LANL2DZ level were shown in Fig. 3. The ground state structure of **PMBTZ** and **PHBTZ** possess twist of 103.4° and 96.0° between the porphyrin macrocycle and the thienyl unit. And the dihedral angles of the thienyl and the BTZ units of the two dyes are 0.9° and −0.3°. Relatively, **PMBTZ** possesses more delocalization over an entire conjugated system than **PHBTZ**. Further, the UV–visible absorption spectra of the two porphyrin dyes adsorbed onto TiO_2 films are described in Fig. 4. Both the two dyes show broad absorption spectra, in the range of 350–800 nm. A slight red-shift from 423 to 442 nm was found due to the *J*-aggregation on TiO_2 electrode. Such a broadening of the absorption spectra is due to an interaction between the dyes and TiO_2 [19]. When the two sensitizers were adsorbed on the TiO_2 electrode, the color of **PMBTZ** based film is darker than that of **PHBTZ**, which predicts more adsorbed amounts. Further, it is obvious that the molar extinction coefficient of **PMBTZ** is larger than that of **PHBTZ** in the range of 350–650 nm when adsorbed on TiO_2 thin film, which is correspondence with the color of the two films. According to the above, **PMBTZ** is expected to gain better IPCE and J_{sc} value.

The fluorescence data of the dyes are listed in Table 1 and the emission spectra is presented in Fig. 5. The fluorescence spectrum of $\mathbf{P_{Zn}}$ exhibits emission with two peaks (λ_{em} = 598, 645 nm) arising from the porphyrin core. The maximum emission peaks of **PMBTZ** and **PHBTZ** are 661 and 656 nm, respectively. And a shift of the maximum fluorescence emission at longer wavelengths is observed as the conjugation increased. Furthermore, the peaks of the two dyes at 598 nm are weaker than that of $\mathbf{P_{Zn}}$, which is accounted for the extent of π-conjugation that causing effective intramolecular electron transfer.

3.3. Electrochemical properties

We employed cyclic voltammetry to determine the redox potentials of the two porphyrins, and the electrochemical reactions of the two dyes were measured in DMF containing 0.1 M tetrabutylammonium hexafluorophosphate as a supporting electrolyte. The cyclic voltagram is shown in Fig. 6 and the electrochemical data are summarized in Table 2. The first oxidation potentials (E_{ox1}) of the two dyes, corresponding to the HOMO energies of the dyes,

Table 1
UV–visible, PL spectral data of porphyrin dyes.

Dyes	Soret/Q-band(s)[a] (ε,$10^5\ M^{-1}\ cm^{-1}$)[a]	Soret/Q-band (f)[b]	Γ[c] /10^{-8} mol cm^{-2}	λ_{em} (nm)[d]	λ_{int} (nm)[e]
PMBTZ	424 (1.19), 571 (0.25)	448, 580	2.4	661, 726	594
PHBTZ	423 (2.35), 552 (0.38)	442, 583	0.85	612, 656	577
$\mathbf{P_{Zn}}$	420 (2.21), 547 (0.07)			598, 645	448

[a] Absorption spectra measured in $CHCl_3$ solution.
[b] Absorption spectra obtained on TiO_2 film.
[c] Amount of the dyes absorbed on TiO_2 film.
[d] Wavelengths for emission spectra in $CHCl_3$ solution by exciting at Soret-wavelength.
[e] Measured by the intercept of the normalized absorption and emission spectra.

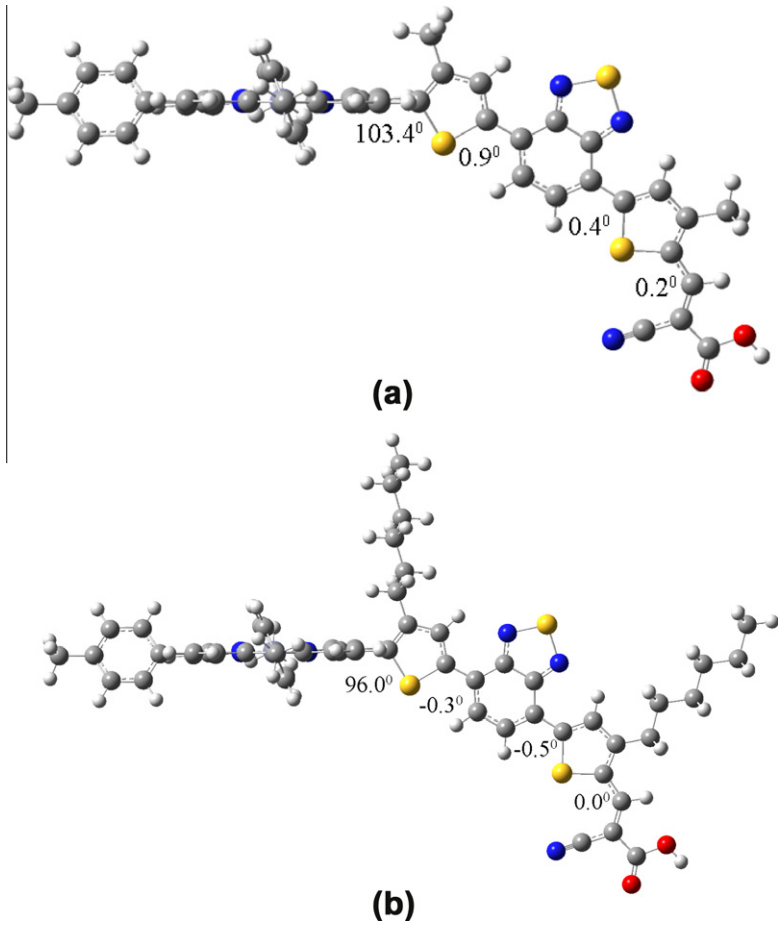

Fig. 3. The optimized structures of (a) **PMBTZ** and (b) **PHBTZ** calculated at density functional B3LYP/LANL2DZ level.

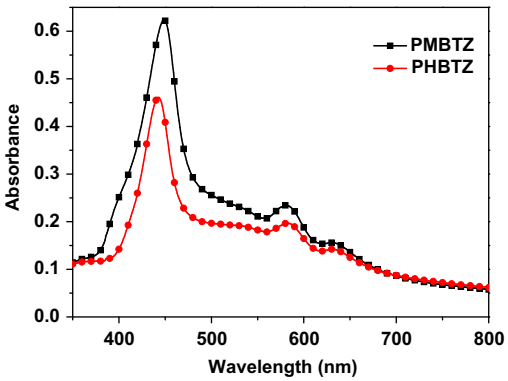

Fig. 4. UV–visible absorption spectra of porphyrins adsorbed on TiO_2 films.

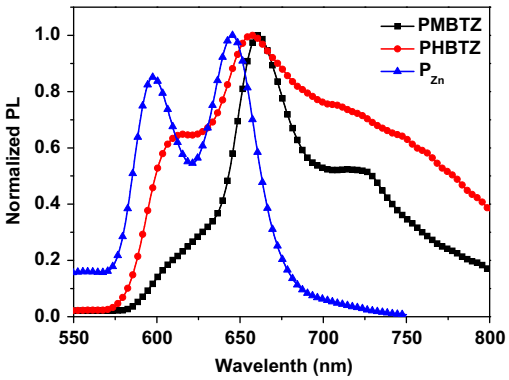

Fig. 5. Normalized PL spectra of porphyrin dyes in $CHCl_3$.

are 1.11 and 1.15 eV, respectively. They are both at potentials greater than that of the I^-/I_3^- couple, which assure regenerations of the oxidized states. The reduction oxidation potentials are obtained from the relation $E_{red} = E_{ox1} - E_{0-0}$, in which E_{ox1} is the first oxidation potential of a porphyrin dye and E_{0-0} is the zero–zero excitation energy obtained from the intersection of absorption and emission spectra the absorption edge [20]. The calculated E^*_{0-0} values are −0.98 and −1.00 eV, respectively. They are both more negative than the conduction edge (−0.50 V vs. NHE) of TiO_2, which is compatible with electron injection from the excited state of the dye to the conduction band (CB) of TiO_2. As described above, the energy levels for the two dyes

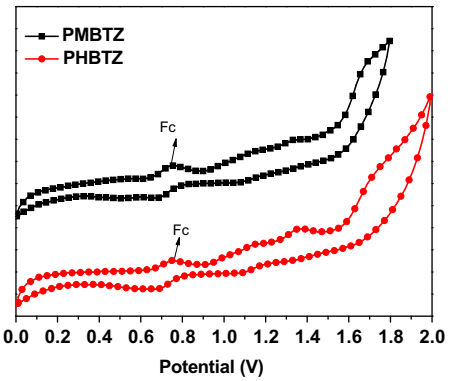

Fig. 6. Cyclic voltammograms of the porphyrin dyes.

Table 2
Electrochemical data for porphyrin dyes and driving forces for electron-transfer processes on the TiO_2.

Dyes	E_{0-0}[a] (eV)	E_{ox1}[b] (V)	E_{red}[c] (V)	ΔG_{inj}[d] (eV)	ΔG_{reg}[e] (eV)
PMBTZ	2.09	1.11	−0.98	−0.48	−0.61
PHBTZ	2.15	1.15	−1.00	−0.50	−0.65
$\mathbf{P_{Zn}}$	2.77	1.230	−1.290		

[a] Determined from the intercept of the normalized absorption and emission spectra.
[b] First oxidation potentials (vs. NHE).
[c] First reduction potentials approximated from E_{ox1} and E_{0-0} (vs. NHE).
[d] Driving forces for electron injection from the porphyrin excited singlet state (E^*_{ox}) to the conduction band of TiO_2 (−0.5 V vs. NHE).
[e] Driving forces for regeneration of the porphyrin radical cation by I^-/I_3^- redox couple (+0.5 V vs. NHE).

both fulfill the requirement for effective electron injection and dye regeneration in a DSSC system.

In order to gain further insight into the molecular orbital spatial distribution, the frontier molecular orbitals of the dyes **PMBTZ** and **PHBTZ** were also simulated based on density functional theory (DFT) calculations at B3LYP/LANL2DZ level. Full geometry optimizations and frequency/intensity calculations of the novel porphyrin sensitizers were performed at B3LYP level using the LANL2DZ basis set. None of the frequency calculations generated imaginary frequencies, indicating that the optimized geometries were true energy minima. All calculations were performed using the Gaussian03 program [22] on the IBM P690 system in the Shandong Province High Performance Computer Center. The spatial distributions of the HOMO and LUMO of the dyes are shown in Fig. 7. It is obvious that the HOMO is localized mainly on the porphyrin cycle and extended along the π-conjugated bridge to the central region of the molecule. On the other hand, the LUMO is localized mainly along the cyanoacrylic unit through thienyl and BTZ units. We notice that the HOMO–LUMO excitation induced by light irradiation could move the electron distribution from porphyrin cycle to the cyanoacrylic acid moiety via thienyl and BTZ bridges, and the photo-induced electron transfer from the dyes to the TiO_2 electrode can occur efficiently by the HOMO–LUMO transition.

3.4. Photovoltaic properties of porphyrin-sensitized TiO_2 cells

The dye-sensitized solar cells were constructed using P25 TiO_2 film based on the two dyes. Details for the fabrication of DSSCs are described in Section 2. The device performance parameters under simulated AM 1.5 irradiation (100 mW cm^{-2}) are collected in Table 3 and the photovoltaic characteristics of DSSCs based on the two dyes are shown in Fig. 8.

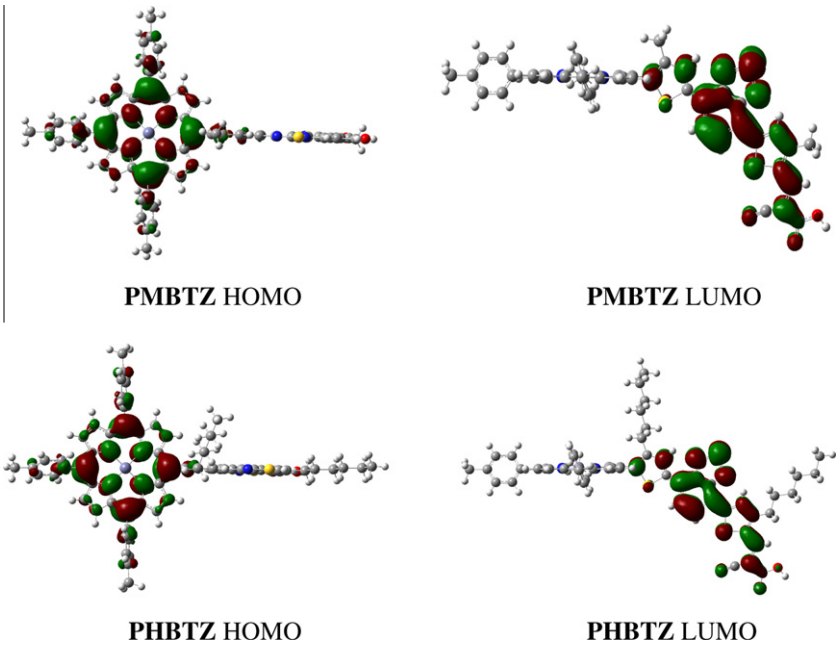

Fig. 7. Molecular orbital spatial distributions of the porphyrin dyes.

Table 3
Photovoltaic performance of DSSCs for the two dyes.

Dyes	J_{sc} (mA/cm^2)	V_{oc} (V)	*ff*	η (%)
PMBTZ	14.11	0.59	0.66	5.46
PHBTZ	10.86	0.61	0.71	4.67

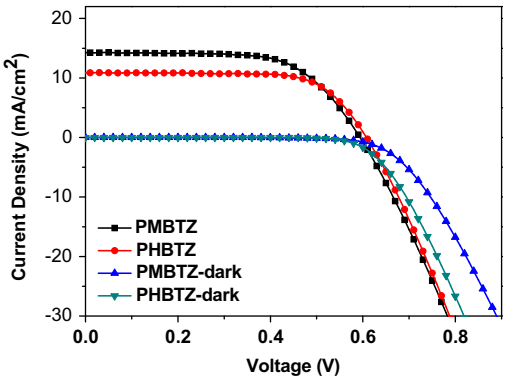

Fig. 8. Current density–voltage characteristics for DSSCs based on the dyes under illumination and dark condition.

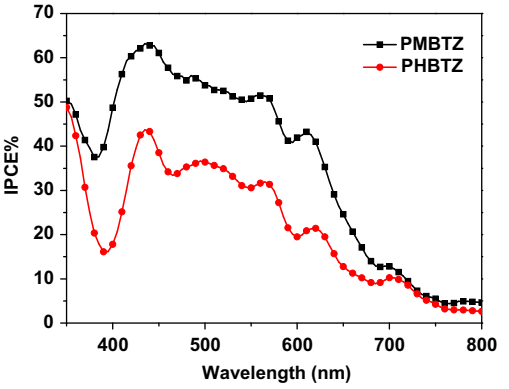

Fig. 9. IPCE plots for the DSSCs based on the two porphyrin dyes.

The incident photo-to-current conversion efficiency (IPCE) plots for the DSSCs based on the two porphyrin dyes are showed in Fig. 9. The two dyes both respond in the broad range of 350–800 nm and show the maximum IPCE values around 440 nm, which is accordant with the spectra of the dyes adsorbed on the TiO_2 films. It's worthy noting that the response of the dyes modified with low-band-gap chromophore in the range of 450–550 nm is much stronger than porphyrin dyes reported by our group previously [11e,21]. Further the IPCE values of **PMBTZ** is much higher than **PHBTZ** in the whole broad range which may be resulted from the bigger Γ value, thus may lead to a relatively larger photocurrent in DSSC. As shown in Table 3, the **PMBTZ**- and **PHBTZ**-sensitized solar cells gave the short circuit photocurrent densities (J_{sc}) of 14.11 and 10.86 mA cm^{-2}, open circuit voltages (V_{oc}) of 0.59 and 0.61 V and the fill factors (*ff*) of 0.66 and 0.71, corresponding to overall conversion efficiencies of 5.46% and 4.67%, respectively. As we expected, the short circuit photocurrent density (J_{sc}) for DSSCs based on **PMBTZ** is larger than that of **PHBTZ** under the same conditions. To demonstrate the absorptivity of the two high molar extinction coefficient sensitizers on thin-film devices, we also determined the adsorbed dye amounts on the thin films. The total amounts (Γ) of the porphyrins adsorbed on the TiO_2 films were determined by measuring the absorbance of the dyes that were dissolved from the dye-modified TiO_2 films into DMF/H_2O = 4:1 containing 0.1 M NaOH. The Γ values of the porphyrins absorption in DMF are listed in Table 1. The adsorbed amounts of **PMBTZ** (**2.4** $\times$ **10**$^{-8}$ mol/cm^2) is larger than that of **PHBTZ** (**0.85** $\times$ **10**$^{-8}$ mol/cm^2), which is correspondence with the absorption spectra of the dyes adsorbed on TiO_2 thin films and the IPCE values discussed previously. The result is attributed to the introduction of the long hexyl chain to the thiophene segment, which blocks the absorption of the dye to the TiO_2 and increases the distances between the adjacent dye molecules.

To gain further investigation of the device performances of the two dyes, a dark current test was conducted. And the current–voltage curves obtained under dark conditions were shown in Fig. 8. The curves showed onsets that were obviously more positive for the DSSCs based on **PMBTZ** than that of **PHBTZ**. It indicates that the back-electron-transfer process corresponding to the reaction between the conduction-band electrons in the TiO_2 and I_3^- ion in the electrolyte occurs more easily under dark condition in DSSCs based on **PHBTZ** than that of **PMBTZ**.

4. Conclusions

In summary, we have developed a new class of porphyrin dyes featuring donor–acceptor architecture that incorporating low-band-gap chromophore. They are successfully adsorbed on nanocrystalline anatase TiO_2 particles, and subsequently efficient dye-senstitized solar cells have been fabricated. As expected, the introduction of the low-band-gap moieties negated the E_{ox1} of the two dyes and narrowed the energy gap, which has positive effect on improving the light-harvest ability of the dyes. The impressive performance dye-sensitized solar cell based on **PMBTZ** exhibits a maximum incident photon-to-current conversion efficiency (IPCE) value of 65%, with a J_{sc} of 14.11 mA/cm2 and a V_{oc} of 0.59 V. Finally, it seems that the modification with the low-band-gap chromophores in the bridge of the porphyrin dyes at meso-position is an effective strategy to improve the spectra. Furthermore, methyls on the thienyls are more effective in reducing the charge recombination of the injected electrons with triiodide ions. The inherent mechanism would be studied in following investigation.

Acknowledgements

This work was supported by the National Nature Science Foundation of China (No. 50973092, 51173154, 21171084), and the National Basic Research Program of China (No. 2011CBA00701), and the Specialized Research

Fund for the Doctoral Program of Higher Education of China (No. 20104301110003).

References

[1] (a) B. O'Regan, M. Grätzel, Nature 353 (1991) 737;
(b) W.D. Zeng, Y.M. Cao, Y. Bai, Y.H. Wang, Y.S. Shi, M. Zhang, F.F. Wang, C.Y. Pan, P. Wang, Chem. Mater. 22 (2010) 1915.

[2] (a) M.K. Nazeeruddin, A. Kay, I. Rodicio, R. Humphrybaker, E. Muller, P. Liska, N. Vlachopoulos, M. Grätzel, J. Am. Chem. Soc. 115 (1993) 6382;
(b) M. Grätzel, J. Photochem. Photobiol. A 164 (2004) 3;
(c) A. Islam, F.A. Chowdhury, Y. Chiba, R. Komiya, N. Fuke, N. Ikeda, K. Nozaki, L.Y. Han, Chem. Mater. 18 (2006) 5178;
(d) M.K. Nazeeruddin, F.D. Angelis, S. Fantacci, A. Selloni, G. Viscadi, P. Liska, S. Ito, B. Takeru, M. Gratzel, J. Am. Chem. Soc. 127 (2005) 16835.

[3] (a) Z.S. Wang, Y. Cui, K. Hara, Y. Dan-oh, C. Kasada, A. Shinpo, Adv. Mater. 19 (2007) 1138;
(b) K. Hara, M. Kurashige, Y. Danoh, C. Kasada, A. Shinpo, S. Suga, K. Sayama, H. Arakawa, New J. Chem. 27 (2003) 783.

[4] B. Liu, W. Zhu, Q. Zhang, W. Wu, M. Xu, Z. Ning, Y. Xie, H. Tian, Chem. Commun. 13 (2009) 1766.

[5] C. Zafer, M. Kus, G. Turkmen, H. Dincalp, S. Demic, B. Kuban, Y. Teoman, S. Icli, Sol. Energy Mater. Sol. Cells 91 (2007) 427.

[6] X. Ma, J. Hua, W. Wu, Y. Jin, F. Meng, W. Zhan, H. Tian, Tetrahedron 64 (2008) 345.

[7] S. Hayashi, M. Tanaka, H. Hayashi, S. Eu, T. Umeyama, Y. Matano, Y. Araki, H. Imahori, J. Phys. Chem. C 112 (2008) 15576.

[8] P. Shen, Y. Liu, X. Huang, B. Zhao, N. Xiang, J. Fei, L. Liu, X. Wang, H. Huang, S.T. Tan, Dyes Pigm. 83 (2009) 187.

[9] D. Liu, B. Zhao, P. Shen, H. Huang, L. Liu, S.T. Tan, Sci. China Ser. B: Chem. 52 (2009) 1198.

[10] V.A. Nuay, D.H. Kim, S.H. Lee, J. Ko, Bull. Korean Chem. Soc. 30 (2009) 2871.

[11] (a) D. Kim, A. Osuka, J. Phys. Chem. A 107 (2003) 8791;
(b) D. Kim, A. Osuka, Acc. Chem. Res. 34 (2001) 40;
(c) H. Yamada, H. Imahori, Y. Nishimura, I. Yamazaki, T.K. Ahn, S.K. Kim, D. Kim, S. Fukuzumi, J. Am. Chem. Soc. 125 (2003) 9129;
(d) T. Hasobe, K. Saito, P.V. Kamat, V. Troiani, H. Qiu, N. Solladie, K.S. Kim, J.K. Park, D. Kim, F. D'Souza, S. Fukuzumi, J. Mater. Chem. 17 (2007) 4160;
(e) Y. Liu, N. Xiang, X. Feng, P. Shen, W. Zhou, C. Weng, B. Zhao, S. Tan, Chem. Commun. 18 (2009) 12499.

[12] T.L. Ma, K. Inoue, H. Noma, K. Yao, E. Abe, J. Photochem. Photobiol. A 152 (2002) 207.

[13] Q. Wang, W.M. Campbell, E.E. Bonfantani, K.W. Jolley, D.L. Officer, P.J. Walsh, K. Gordon, R. Humphry-Baker, K. Nazeeruddin, M. Grätzel, J. Phys. Chem. B 109 (2005) 15397.

[14] S. Eu, S. Hayashi, T. Umeyama, Y. Matano, Y. Araki, I.H. Mahori, J. Phys. Chem. C 112 (2008) 4396.

[15] W.M. Campbell, K.W. Jolley, P. Wagner, K. Wagner, P.J. Walsh, K.C. Gordon, L. Schmidt-Mende, M.K. Nazeeruddin, Q. Wang, M. Grätzel, D.L. Officer, J. Phys. Chem. C 111 (2007) 11760.

[16] (a) C.W. Lee, H.P. Lu, C.M. Lan, Y.L. Huang, Y.R. Liang, W.N. Yen, Y.C. Liu, Y.S. Lin, E.W.G. Diau, C.Y. Yeh, Chem. Eur. J. 15 (2009) 1403;
(b) T. Bessho, S.M. Zakeeruddin, C.Y. Yeh, E.W.G. Diau, M. Grätzel, Angew. Chem. Int. Ed. 49 (2010) 1.

[17] (a) R. Ma, P. Guo, H. Cui, X. Zhang, M.K. Nazeeruddin, M. Grätzel, J. Phys. Chem. A 113 (2009) 10119;
(b) R. Ma, P. Guo, L. Yang, L. Guo, X. Zhang, M.K. Nazeeruddin, M. Grätzel, J. Phys. Chem. A 114 (2010) 1973;
(c) R. Ma, P. Guo, L. Yang, L. Guo, Q. Zeng, G. Liu, X. Zhang, J. Mol. Struct. Theochem 942 (2010) 131.

[18] (a) M. Velusamy, K.R. Justin Thomas, J.T. Lin, Y.-C. Hsu, K.-C. Ho, Org. Lett. 10 (2005) 1899;
(b) Q.M. Zhou, Q. Hou, L.P. Zheng, X.Y. Deng, G. Yu, Y. Cao, Appl. Phys. Lett. 84 (2004) 1653;
(c) C.J. Brabec, C. Winder, N.S. Sariciftci, J.C. Hummelen, A. Dhanabalan, P.A. Van Hal, R.A. Janssen, Adv. Funct. Mater. 12 (2002) 709;
(d) C. Winder, N.S. Sariciftci, J. Mater. Chem. 12 (2004) 1077;
(e) E. Bundgaard, F.C. Krebs, Sol. Energy Mater. Sol. Cells 91 (2007) 954;
(f) E. Bundgaard, F.C. Krebs, Macromolecules 39 (2006) 2823.

[19] K. Hara, M. Kurashige, Y. Dan-oh, C. Kasada, A. Shinpo, S. Suga, K. Sayama, H. Arakawa, New J. Chem. 27 (2003) 783.

[20] (a) D.P. Hagberg, J.-H. Yum, H. Lee, F.D. Angelis, T. Marinado, K.M. Karlsson, R. Humphry-Baker, L. Sun, A. Hagfeldt, M. Grätzel, M.K. Nazeeruddin, J. Am. Chem. Soc. 130 (2008) 6259;
(b) J.K. Park, H.R. Lee, J. Chen, H. Shinokubo, A. Osuka, D. Kim, J. Phys. Chem. C 112 (2008) 16691.

[21] N. Xiang, X. Huang, X. Feng, Y. Liu, B. Zhao, L. Deng, P. Shen, J. Fei, S.T. Tan, Dyes Pigm. 88 (2011) 75.

[22] M.J. Frisch et al., Gaussian'03, Revision B 05, Gaussian Inc., Pittsburgh, PA, 2003.